

International Journal of Research Publication and Reviews

Journal homepage: www.ijrpr.com ISSN 2582-7421

ENVIRONMENTAL IMPACT ASSESSMENT OF CONTINUOUS USE OF FERTILIZER IN UPLAND FARMLAND, OGHARA, DELTA STATE USING INTEGRATED GEOPHYSICAL AND PHYSICOCHEMICAL METHODS

Umuze M. Walter¹, Idiegbe O. Gilbert²

1.2 Physics Unit, Department of Science Laboratory Technology,Delta State Polytechnic,Otefe – Oghara, Nigeria

ABSTRACT:

This research carried out the integration of electromagnetic, 1-D, 2-D and 3-D electrical resistivity geophysical methods combined with Physicochemical methods were investigated to understand the level of pollution on soil and groundwater as a result of the use of fertilizers in Upland farmlands in Delta State, Niger-Delta, Nigeria. A total of twenty seven (27) very low frequency (VLF) and 2-D electrical resistivity imaging (ERI) traverses were acquired with in a grid format in upland with one control traverse within the study area. Twenty-four (24) VES readings were conducted and one (1) VES as control (1) kilometre away from the project site). Physicochemical investigation involving physical and chemical analyses of three (3) water samples taken from three different existing boreholes and three (3) soil samples were collected within the study area for groundwater, soil and fertilizer leachate analysis. Karous - Hjelt filter software was used to process the VLF data while RES2DINV and RES3DINV software's were used to process and inverted the 2-D and 3-D depth slice resistivity data. The 3-D cubic model was processed using the ZondRES3D software. The WINRESIST (1.0) geophysical software was used for analysis of the VES data. Anthropogenic pollution determinants parameters such as pH, conductivity, total dissolved solids, cations, anions and the less abundant heavy metals such as cadmium, copper, iron, manganese, lead and coliform count were analysed and other parameters based on WHO standards using the APHA, ASIMD and ASTID methods. The results of very low frequency (VLF) show area of low and high conductive zones. The real and imaginary component of the VLF ranges from -2 -to +6 and -2 to +20 indicating high conductive fertilizer contaminants region. The inverted VLF 2D conductivity structure reveals the movements of fertilizer contaminants downwards within the area of study. The fertilizer leachate was more confined across the study areas at about $0-15\,\mathrm{m}$ and $0-30\,\mathrm{m}$ depth and with conductivity values of +10 to +20 msec. The 2-D inverted resistivity structures also show movements of fertilizer contaminants laterally and vertically within both study area of investigation. The fertilizer contamination plume was pronounced across the study areas at about $0-39.6\,\mathrm{m}$ and $1.25-19.8\,\mathrm{m}$ depth and having resistivity values ranging from $44-49\Omega m$.

Keywords: Fertilizer, contaminants, farmland, Oghara and soil

INTRODUCTION

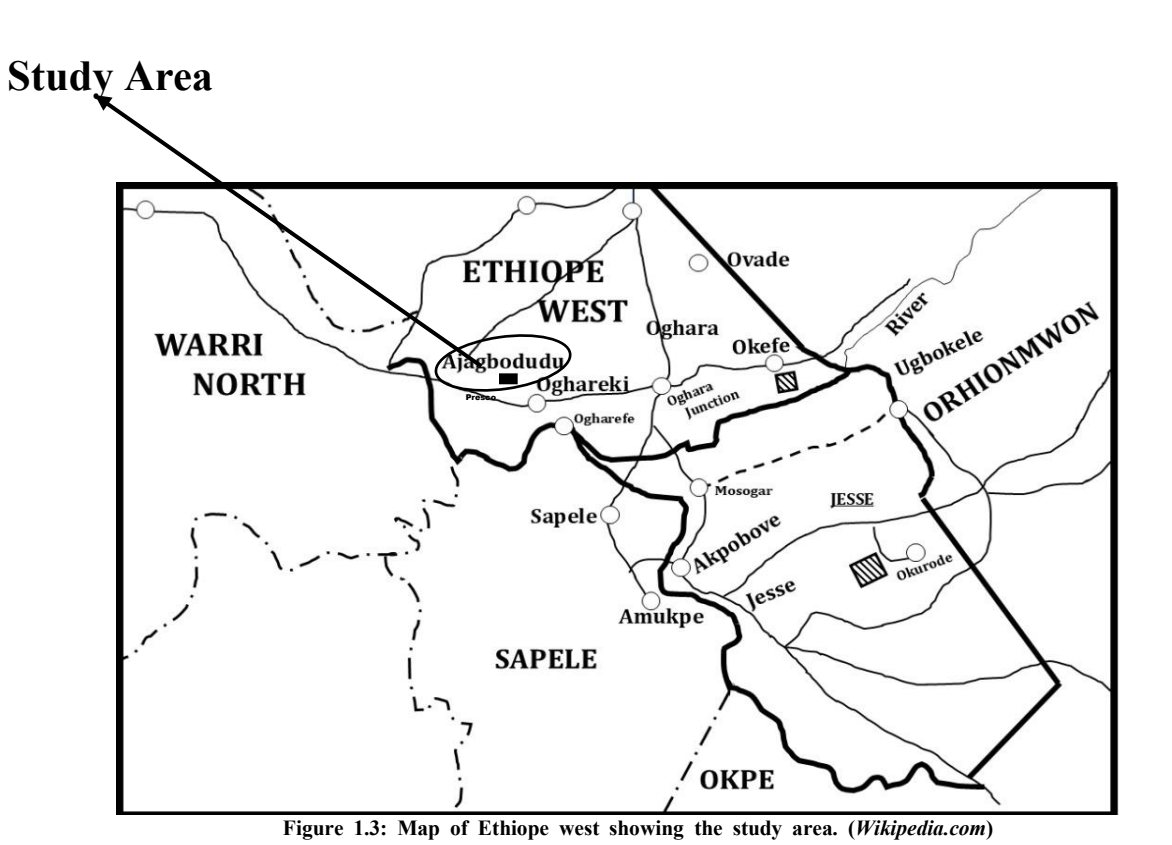
Fertilization increases efficiency and obtains better quality of product recovery in agricultural activities. It is one of the most important ways. Nonorganic fertilizers mainly contain phosphate, nitrate, ammonium and potassium salts. Fertilizer industry is considered to be source of natural radio-nuclides and heavy metals as a potential source. It contains a large majority of the heavy metals like Hg, Cd, As, Pb, Cu, Ni, and Cu; natural radionuclide like ²³⁸U, ²³²Th, and ²¹⁰Po (FAO, 2009; Sönmez*et al.*, 2007). However, in recent years, fertilizer consumption increased exponentially throughout the world, causes serious environmental problems. Fertilization may affect the accumulation of heavy metals in soil and plant system. Plants absorb the fertilizers through the soil, they can enter the food chain. Thus, fertilization leads to water, soil and air pollution. Fertilizers play a vital role in modern agriculture, significantly increasing crop yields and feeding a growing population. However, it is important to understand the potential environmental impacts associated with their use.

Soil is a very important and sensitive resource of a nation. In order to meet increasing public needs and to promote crop products, the use of high inputs of chemicals in the soil in the form of fertilizers, pesticides, fungicides, insecticides, nematicides and weedicides, along with intensive irrigation practices, helped to achieve the target to a certain stage. However, the decrease in crop yield took place despite the application of fertilizer. The toxic chemicals influence the life of beneficial soil microorganisms, which are indeed responsible for maintaining soil fertility. Moreover, groundwater, air, and human and animal health have also been adversely affected by these chemicals directly and indirectly.

For the purpose of this study, the Environmental Impact Assessment (EIA) of the Effect of continuous use of fertilizers on the earth's subsurface investigated using Very Low Frequency (VLF), 2D and 3D geoelectrical resistivity imaging and physicochemical analyses of soil and water samples were employed in order to map and access the degree of fertilizer contamination at Upland farmland in Oghara, Delta State, South-South, Nigeria.

Local geology of the study area

The study was carried out in the mangrove swamp of Delta State, which lies between within longitudes 005° 36' 12.80" E to 005° 36' 17.41" E, latitudes 06° 0' 29.13" N to 06° 0' 36.08" N and elevation of 6 to 18 m in Upland farmland. The selected farmland is situated at Oghara, Ethiope West Local Government Area, Delta State. Rainfall occurs mainly between April and October. Annual rainfall is usually between 2000mm- 3000mm with an intense sunlight, which lasts for a mini-mum of 8 hours daily. Temperatures are high for most parts of the year, especially in the months of November to April with a mean monthly of 31°C. The annual range of temperature is thus small only varying between 3°C and 5°C. Relative humidity varies from 90% during rains to about 60% in dry season (Iloeji, 2003). There are three types of soils in Delta state. These consist of alluvial soils on the marine deposits along the coast, alluvial and hydro-morphic soils on marine and lacustrine deposits found in the area close to the Niger and Benin Rivers and the feral soils on loose sandy sediments in the dry land area of the north and north east (Iloeji, 2003; Umeri *et al.*, 2016).



METHODOLOGY

Materials

The data was acquired using the following equipment and accessories;

Clean plastic water bottle, Soil auger, Geonie VLF Terrameter, PASI 16GL model Electrical Resistivity Meter, Twenty-one metal electrodes, Four hammers for driving the electrodes in the ground , Crocodile clips, Two measuring tapes for measuring the distances for the different electrode spacing , Global Positioning System 12 (GPS) for finding the position and elevation of the survey point , Power supply- 12V 60Ah battery, Umbrella, Four reels of red and blue colored electric cable, Base map and, Data sheet for recording the field data

Methods

Theory of work: VLF-EM survey

The skin depth (δ) determines how deep VLF signals penetrate before attenuating:

$$\delta = \sqrt{\frac{2}{\omega\mu\sigma}} \tag{1}$$

• Where: $\omega = 2\pi f$ = Angular Velocity (rad/s), f = VLF transmitter frequency, $\mu = \mu_0 \mu_r$ = Magnetic permeability (H/m), and σ = Electrical conductivity (S/m)

The tilt angle (α) measures the distortion of the magnetic field due to subsurface conductors:

$$\tan \alpha = \frac{H_z}{H_x} \tag{2}$$

• Where: H_z = Vertical component of the secondary magnetic field and H_x = Horizontal component of the primary magnetic field. The phase difference (φ) between the primary and induced secondary fields helps identify conductors:

$$\phi = tan^{-1} \left(\frac{lmaginary (Quadrature)}{Real (In-Phase)} \right)$$
 (3)

Theory of work: Electrical Resistivity

Single Electrode Potential:

$$V_r = \frac{\rho I}{2\pi} \cdot \frac{1}{r} \tag{4}$$

Two Electrodes (Source & Sink):

$$\delta V_{MN} = \frac{\rho I}{2\pi} \left\{ \left[\frac{1}{AM} - \frac{1}{MB} \right] - \left[\frac{1}{AN} - \frac{1}{NB} \right] \right\} \tag{5}$$

Apparent Resistivity (ρ_a):

$$\rho_a = R \times K \tag{6}$$

• $R = \Delta V/I$ (Resistance)

• K = Geometric factor (depends on array configuration)

Wenner Array:

$$K = 2\pi a$$

$$\rho_a = 2\pi a \frac{\Delta V}{I}$$
(7)

(8)

Schlumberger Array:

$$K = \frac{\pi L^2}{2L} \tag{9}$$

$$\rho_a = \frac{\pi V}{4I} \left(\frac{L^2 - a^2}{a} \right) \tag{10}$$

Data Acquisition

1. Very Low Frequency (VLF)

A total of thirteen (13) traverses were acquired in a grid format, thirteen (13) traverses in site and one (1) traverse serves as control profile.

2. Two-dimensional (2D) resistivity imaging

A total of thirteen (13) 2D traverses were acquired in a grid format and one (1) traverse serves as control profile. The Wenner array electrode was used for the 2D resistivity imaging data acquisition. This electrode configuration is well suited for constant separation data acquisition systems, so that many data-points can be recorded simultaneously for each current injection. A 2D resistivity survey was carried out using the PASI Resistivity meter. Measurements were made at sequences of electrodes at 10m, 20m, 30m, 40m, 50m and 60m interval using four (4) electrodes for all the traverses covering a distance of 200m each.

3. Schlumberger Array

The Schlumberger electrode array configuration was used and the current electrode separation (AB) was varied from a minimum of 2 to 200m. Twenty-three (2) VES stations were acquired and one (1) VES serves as control at different points. The geodetic system of coordinates was obtained using Garmin 12 GPS. Electrodes were driven into the ground using the hammer till good contact was made to the ground. The current and voltage electrodes were placed to the ground and connected to the resistivity meter via the reels of purple electric cables respectively using alligator clips so as to make good connection. Current was supplied to the current electrodes by the terrameter and the corresponding values of the resistivity, voltage and current were read off on the PASI resistivity meter and recorded. The cables were checked after each VES data was acquired. GPS readings were taken in all the VES points.

4. Soil Sampling

Soil samples were taken from three (3) locations within thestudy areas using the soil auger. Two (2) from the affected area and one (1) far from the unaffected area which serves as control sample. The soil samples were taken at depth of 0 to 10 cm, 10 to 25 cm and 25 to 30 cm respectively. The topsoil was removed up to the depth of 15 cm and then the soil beneath was taken; this was repeated for subsequent sampling points.

5. Water Samples Collection

The location coordinates of the three (3) water sample points were collected from the study area. Two (2) from the affected area and one (1) far from the unaffected area which serves as control sample. The samples were collected using one litre of cleaned plastic bottle for each and then sealed. Well (W1) and Well (W2) at Upland farmland, were taken with a Global Positioning System (GPS). Water sample

was collected from a borehole at 45 m deep located at the northern, northwestern and southwestern part of the area. The physical parameter observed in the field was the colour of the water. The collected samples were not preserved due to the fact that the samples were sent directly to the laboratory for analysis. The water samples were filtered to remove suspended particulates from the samples before analysis.

Data Processing/Interpretation

1. Electromagnetic (EM) Method- VLF

The real and imaginary VLF data were inputted in excel sheet and saved in .dat format. This data was then read with the Karous-Hjelt software to generate the 2-D conductivity image of the subsurface. Emphasis is therefore placed on the Fraser filtered plot which helps to transform genuine cross-over points in peaks and the pseudo section produced, by using Karous-Hjelt software. The inversion of the Fraser filtered curve into current density section provides more information as regards the dimension and depth extent of the conductive zones. High conductive zones are displayed in yellow to red color, while the low current density is depicted in green to blue color. The two most used methods for processing VLF-EM data are Fraser and Karous-Hjelt filtering (Fraser, 1969; Karous and Hjelt, 1983).

2. 2-D and 3-D Electrical Resistivity Imaging

The apparent resistivity values for each traverse were collated in a format that is acceptable by the RES2DINV inversion code. Elevation corrections were not included in the measurements as the area surveyed was more or less flat. RES2DINV computer code (Loke and Barker 1996a) was used in the inversion of the 2D data. The computer program uses a nonlinear optimization technique which automatically determines a 2D resistivity model of the subsurface for the input apparent resistivity data (Griffiths and Barker 1993; Loke and Barker 1996a). The program divides the subsurface into a number of rectangular blocks according to the spread of the observed data. Least-squares inversion with standard least-squares constraint which attempt to minimize the square of the difference between the observed and the calculated apparent resistivity values was used to invert all the 2D traverses. The smoothness constraint was applied to the model perturbation vector only. The sensitivity values provide information on the section of the subsurface with the greatest effect on the measured apparent resistivity values. The sensitivity values were normalized by dividing the calculated sensitivity values with the average sensitivity for the particular model configuration. Line search which uses quadratic interpolation to find the optimum step size for the change in apparent resistivity of model blocks was used at each iteration step. Standard Gauss-Newton optimization method was used, with a convergent limit of 0.005. The Jacobian matrix was recalculated for all iterations; homogeneous half-space was used as initial model. A grid size of 4 nodes per unit electrode and normal mesh were used in the forward modelling subroutine for calculating apparent resistivity values. The initial and minimum damping factor used for the inversion is 0.225 and 0.05, respectively (the default setting is 0.160 and 0.015, respectively). The damping factor was allowed to increase with depth by a factor of 1.05 since the resolution of resistivity decreases exponentially with depth. The damping factor was optimized so as to significantly reduce the number of iterations required for convergence, however, the time taken per iteration increases. The entire square set of 2D lines (10 traverses) for Upland farmland were merged together to form a single 3D data set. This was done by collating the measured 2D data (apparent resistivity values) to a 3D data format that can be read by the RES3DINV software (Loke and Barker 1996b) using the RES2DINV computer code. The coordinates, line directions, number of electrodes, electrode spacing and data levels of each of the 2D traverses were used in collating the apparent resistivity values with the aid of an input text file which can be read by the computer code. The collated 3D data sets were inverted using RES3DINV computer code which automatically determines a 3D model of resistivity distribution using apparent resistivity data obtained from a 3D resistivity imaging survey (Li and Oldenburg 1994; White et al. 2001). Ideally, the electrodes used for such a survey are arranged in squares grids. The inversion routine used by the RES3DINV program is based on the smoothness constrained least-squares method (de Groot-Hedlin and Constable 1990; Sasaki 1992), as in RES2DINV for 2D inversion, though a robust inversion can also be implemented. The program allows users to adjust the damping factor and the flatness filters in the equation above to suit the data set being inverted. Initial damping factor of 0.215 was used to invert the collated 3D apparent resistivity data set. After each iterating process, the inversion subroutine generally reduced the damping factor used; a minimum limit (one tenth of the value of the initial damping factor used) was set to stabilize the inversion process. The damping factor was optimized so as to reduce the number of iterations the program requires to converge by finding the optimum damping factor that gives the least RMS error; however, this increases the time taken per iteration. In order to determine the 3D distribution of the model resistivity values from the distribution of apparent resistivity values, the subsurface was subdivided into a number of small square blocks. The program defuncts for the first layer thickness based on the maximum depth of investigation of the array was used and was increased by 1.15 (15%) for subsequent layers. Finite difference grids of three nodes between adjacent electrodes were used. Homogeneous earth model was used as the initial model in the inversion carried out.

3. Vertical Electrical Sounding

Qualitative and Quantitative Analyses

The qualitative interpretation of the depth sounding curves was carried out based on distinctive geo-electric characteristics on the number of layers represented by the four types of the auxiliary curves (H, K, A, and Q). The quantitative interpretation of the depth sounding curves was carried out by adopting the partial curve matching technique (Bhattacharya and Patra, 1968). In order to do this, the VES data were plotted on a transparent overlay. The partial curve matching technique involved the use of a standard two (2) layer master curve and four (4) auxiliary type curves (H, K, A, and Q). This procedure required segment-by-segment curve matching starting from the position with shorter electrode spacing and moving towards those with longer spacing.

The results of the VES curves obtained from the partial curve matching were then used to constrain the interpretation by the computer using iteration software known as WINRESIST. This invariably reduces overestimation of depths. The result of the computer iteration shows the quantitative analysis to know the resistivity, thickness and depth.

Generation of Geoelectric Sections

The geoelectric sections were generated using AUTOCAD software from the VES curves obtained from the WINRESIST Software. This involved the combination of two or more interpreted VES results along a profile.

4. Soil Analysis

Soil samples were taken to the laboratory for comprehensive analysis. 2g of the sample was taken into 250 ml conical flask, 10 ml dichloromethane was added and the mixture was placed on the shaker and shaked for 45 mins. It was transferred to an ultrasonic bath for extraction for 2 hrs. The extract was treated by packing a column containing anhydrous sodium sulphate and silica gel to remove from water and impurities as from the analyses of interest. It was then concentrated to 2 ml in avails bottle ready for gas chromatography analysis. The model gas chromatography used for the analysis Agilent Technologies 6890 coupled with mass spectrometer detector of Agilent Technologies 5975. The principles are separation techniques, these techniques comprise of two phases, the stationary and the mobile phase. The stationary phase is the column with length 30 m, internal diameter 0.320 mm, the thickness is 0.25 micrometer while the mobile phase helium gas the volume of sample injection volume is 1 micro liter. The oven temperature program the initial temp. 60 degrees to hold for 2 mins @ 6 degrees per min to temperature of 300 degrees to hold for 20 mins. The mode is split less.

5. Water Analysis

For concentration of total heavy metal analysis, sample was digested in 250 ml conical flask by adding 30 ml of aqua regia and heated on a hot plate until volume remains about 7-12ml. This is to enable the sample to be efficient for further processes. The digest was filtered using what-man filter paper and the volume made up to the mark in a 50ml volumetric flask, and was then stored in a plastic container for Atomic Absorption Spectrophotometer (AAS) analysis by thoroughly mixing the sample through shaking and 100 ml of it transferred into a glass beaker of 250ml volume. The sample was aspirated into the oxidizing air-acetylene flame or nitrous oxide acetylene flame to facilitate absorption of radiation by atomic species during flame reactions. When the aqueous sample was aspirated, the sensitivity for 1% absorption was observed.

RESULTS AND DISCUSSION

Very Low Frequency Em Method (VLF) - Upland Farm Land 1. 2-D Conductivity Section along Traverse 1 - Up Land Farm

A feature at 49 - 58 m and 95 - 109 m is recognized by the agglomeration of the Fraser filter spike and the Karous-Hjelt current concentration. This shallow response indicates a conductive body generated by fertilizer leachates. The geophysical results support this interpretation. The geophysical results also indicate a pollution zone in the shallow sub-surface. The anomaly is declining in intensity from the center over an area consistent with a localized effect.

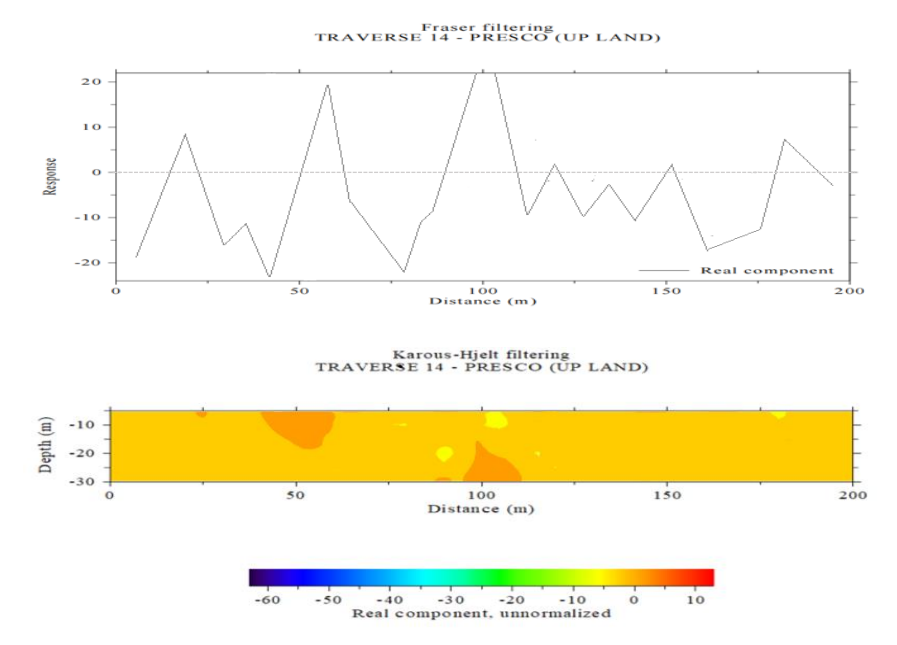


Figure 2: 2-D Conductivity Section along Traverse 1 Up Land Farm

2. 2-D Conductivity Section along Traverse 6 - Up Land Farm

Both the Fraser and Karous-Hjelt filters illustrate a clear conductive anomaly at 25 - 32 m along the traverse in shallow depths (0 - 15) m). The unique response with both filters indicates a conductive feature at that location in the soil profile both images provide enough evidence to interpret lasting pollution-related plume and that is increased because it is very shallow in the profile and is not deep over the shallow depth.

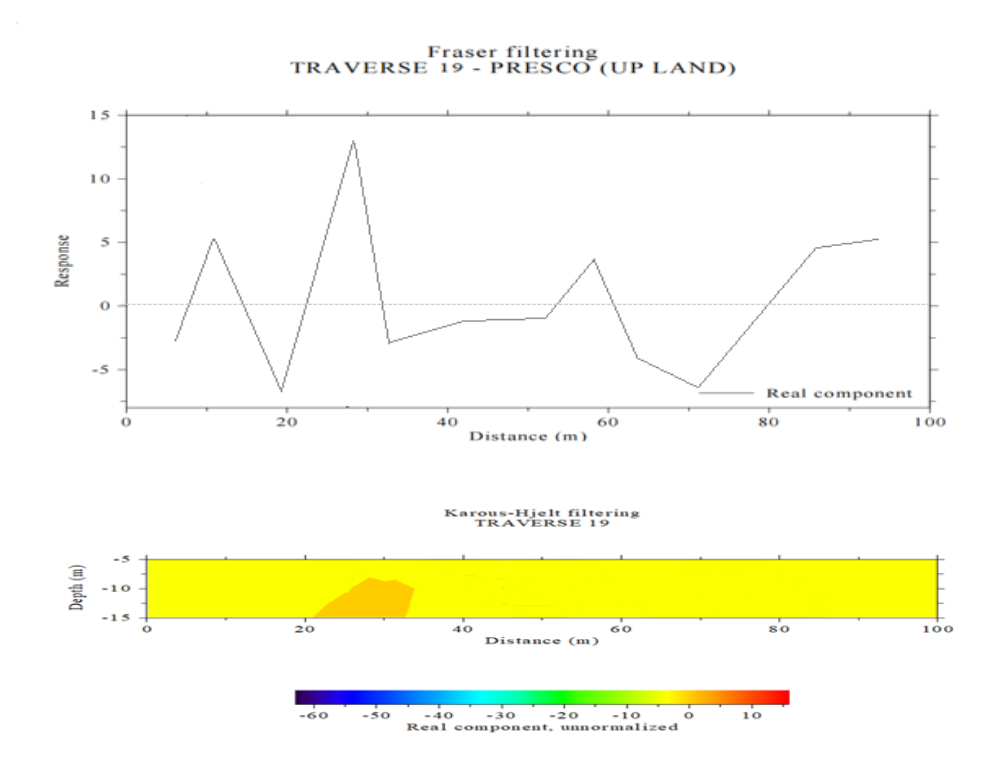


Figure 3: 2-D Conductivity Section along Traverse 6 Up Land Farm

3. 2-D Conductivity Section along Traverse 7 - Up Land Farm

Both the Fraser and Karous-Hjelt filters emphasize a significant conductive anomaly centred at about 5 – 28 m, 40 – 56 m and 74 – 77 m along the traverse but at shallow depths (15 m or less). This aspect has an evident maximum in the Fraser curve and a localized shallow conductive body in the Karous-Hjelt pseudo-section, which validates its geophysical soundness. The aberration indicates that there is greater subsurface conductivity normally attributed to pollution through migration of leachates. The pre-eminence of this feature as compared to lesser anomalies elsewhere qualifies continuous use of fertilizer as the main indicator of contamination along the traverse. Its superficial manifestation indicates that the pollution process is under development and confined to near surface horizons to a great extent. The anomaly disappears laterally and in a depth in the sense that the leachate plume is narrow and not extensive at this traverse.

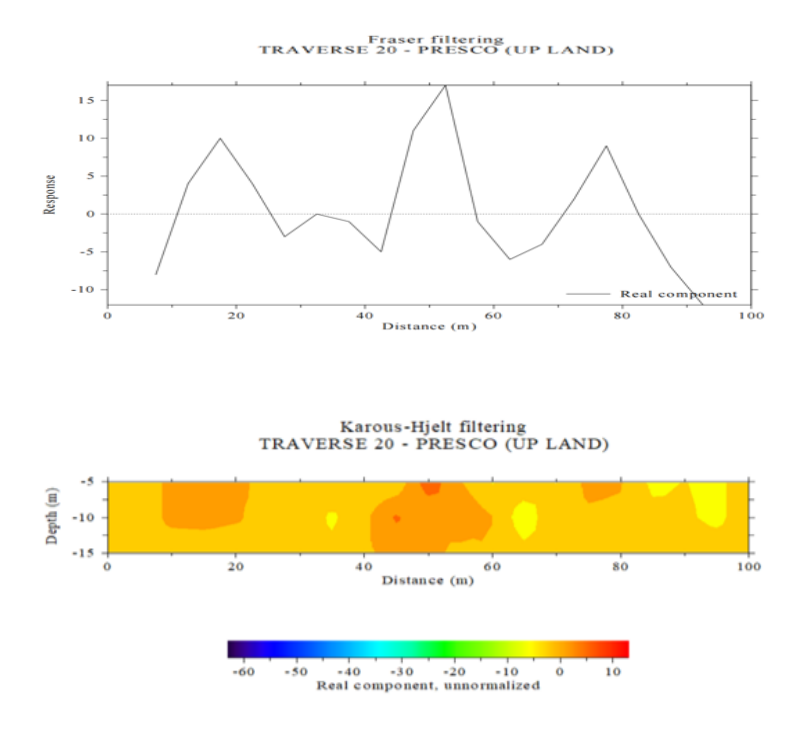


Figure 4: 2-D Conductivity Section along Traverse 7 Up Land Farm

4. 2-D Conductivity Section along Traverse 14 - Control

The Karous-Hjelt pseudo-depth section for the control profile shows an almost consistent subsurface response, with the background in yellow representing moderate to resistive and relatively unaffected conditions. The anomalies identified during the farmland survey as being more conductive with increased resistivity were not observed here in the control section. Only a few wider-spaced pale green patches show some inconsistent deviation from the background between 35-40 m, 55-65 m, and near 75-85 m, which occur at a depth of about 5-12 m. These deviations are marginally visible and are weak and isolated and do not indicate significant conductive features.

The absence of strong orange or red anomalies suggests that the control site is relatively unaffected by fertilizer-derived leachates or ion accumulation. The uniform resistivity of the majority of the section reflects the natural soil and subsurface conditions with no significant evidence of conductive pollution. This provides a reliable baseline to compare fertilizers-impacted farmland sections against.

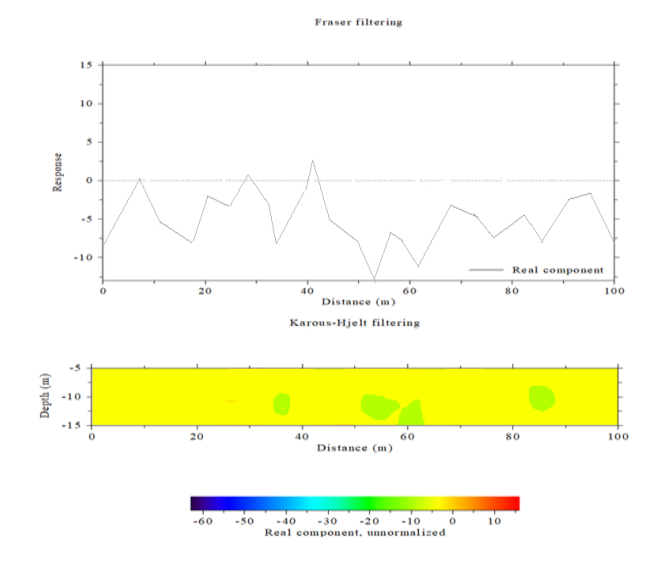


Figure 5: 2-D Conductivity Section along Traverse 14 Control

Discussion of Ert Resistivity Method - Up Land farmland

1. Discussion of ERT along Traverse 1

The 2-D resistivity pseudo-section along traverse 1 is presented in Figure 6. The resistivity of the section varies from $19-2558~\Omega m$ and penetrated to depth of 39.6 m beneath the surface. This profile line showed possible contamination at lateral distance of 0-40~m, 45-58~m and 91-106~m. However, the contamination is observed to have resistivity values ranging from $32-58.3~\Omega m$ and depth ranges from 6.3-13.2~m.

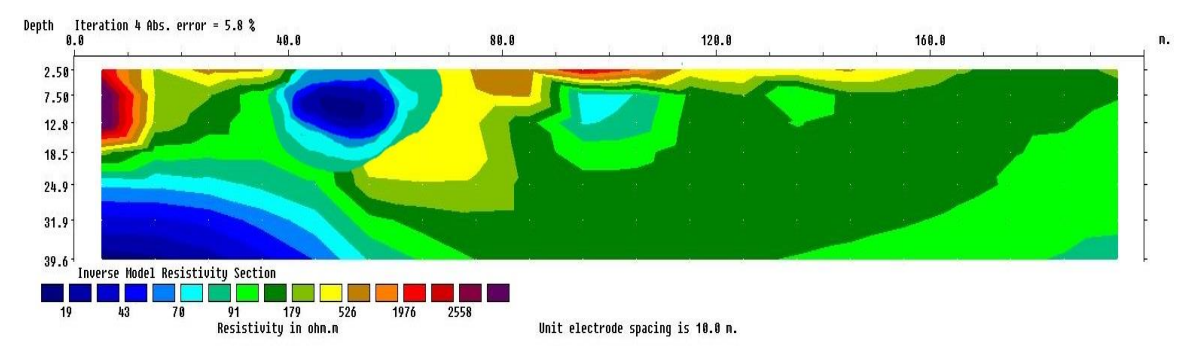


Figure6: 2-D ERT Result along Traverse 1

2. Discussion of ERT along Traverse 6

Figure 7 represents the 2-D resistivity pseudo-section along traverse 6 which covered a total spread length of 100 m. The resistivity of the section varies from $50 - 2785 \,\Omega m$ and penetrated to depth of 19.8 m beneath the surface. The traverse showed possible contamination of the underlying soil resulting to low resistivity at lateral distance of $25.4 - 39.5 \, m$. The resistivity values of this contaminated zone or layer ranges from $50 - 75 \,\Omega m$ and extend from depth range of about $0 - 6.1 \,m$.

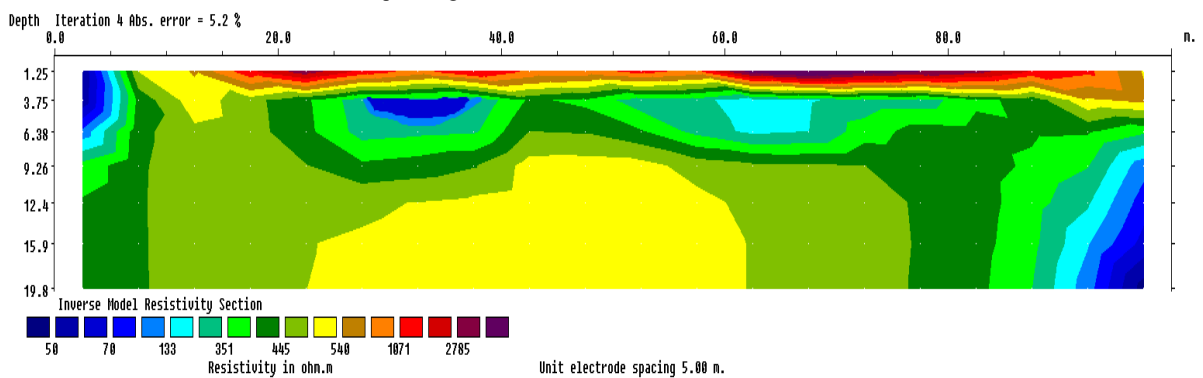


Figure 7: 2-D ERT Result along Traverse 6 - Up Land

3. Discussion of ERT along Traverse 7

The 2-D resistivity pseudo-section along traverse 7 is presented in Figure 8. The resistivity of the section varies from $24 - 1499 \Omega m$ and penetrated to depth of 19.8 m beneath the surface. From the ERT result, possible contamination was identified at lateral distance of 37.8 - 54.3 m having resistivity values ranging from $25 \Omega m - 48 \Omega m$ and extends from the depth of 4 - 9.2 m.

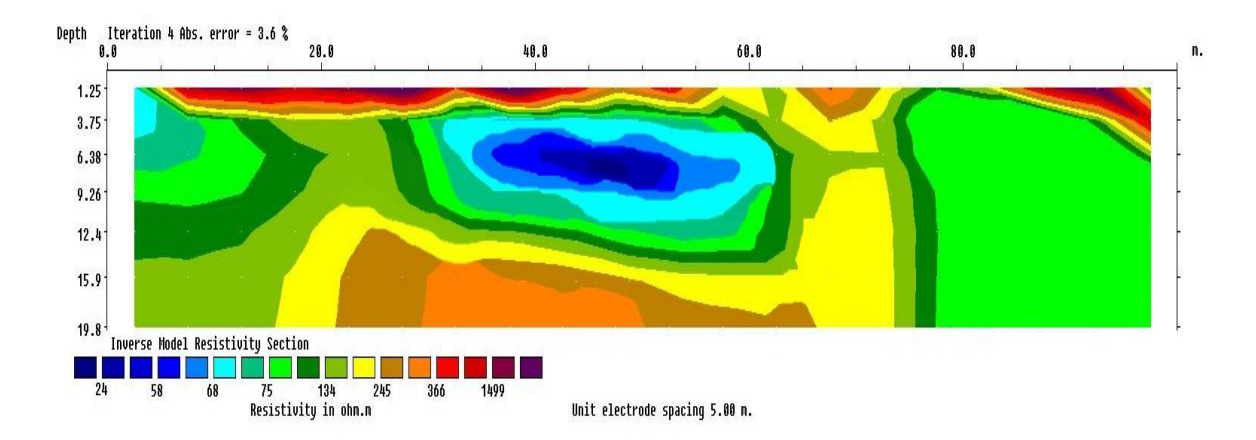


Figure 8: 2-D ERT Result along Traverse 7

4. Discussion of ERT along Traverse 14 - Control

Figure 9 represents the 2-D resistivity pseudo-section along traverse 14 which covered a total spread length of 100 m. The resistivity of the section varies from $186 - 4121 \, \Omega m$ and penetrated to depth of $19.8 \, m$ beneath the surface. The ERT section revealed that the subsurface is composed of sand and extends to depth of $19.8 \, m$. The traverse showed no contamination.

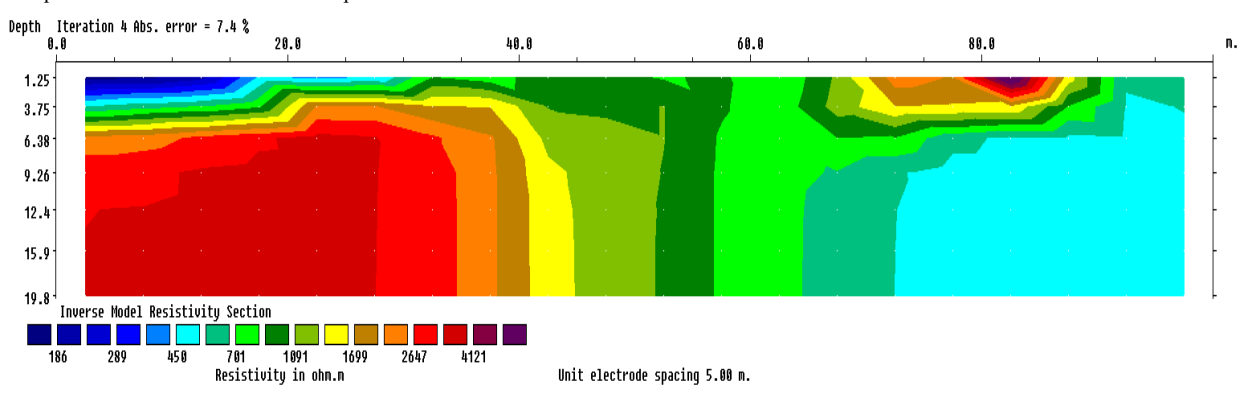


Figure 9: 2-D ERT Result along Traverse 14 - Control

Integration of Results of VLF and ERT Methods-Upland Farmland

1. Correlation of EM-VLF and 2-D Resistivity along Traverse 1 - Up Land $\,$

The contamination was identified at two (2) zones at lateral distance of 45 - 58m and 91 - 106m. The resistivity of these contaminated zones ranges from $32 - 58.3~\Omega m$ and their depth ranges from 6.3 - 13.2m

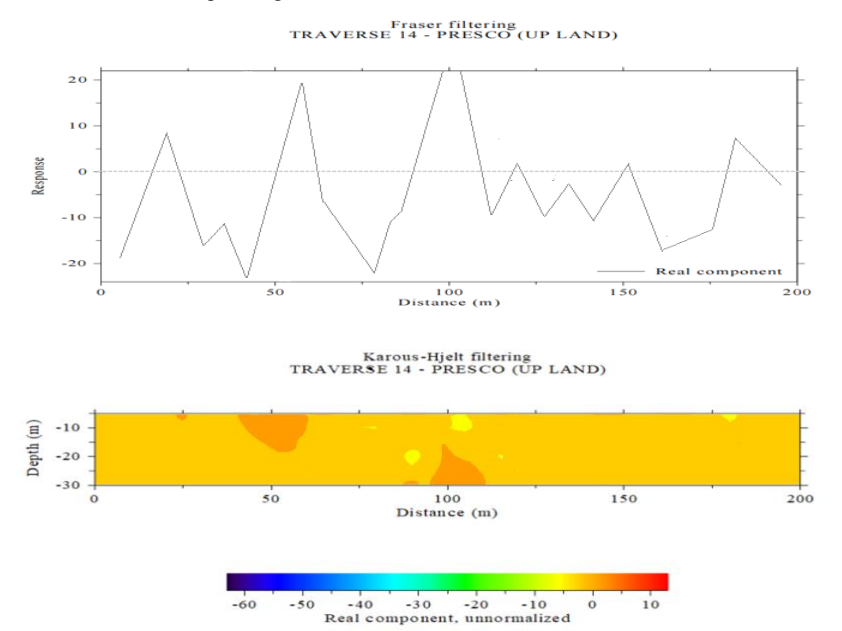


Figure 10: Correlation of VLF Conductivity and ERT Methods along Traverse 1

2. Correlation of EM-VLF and 2-D Resistivity along Traverse 6 - Up Land

The VLF conductor, outlined around 21-33 m on the Karous-Hjelt profile, corresponds clearly with a low-resistivity zone on the ERT image. This conductive anomaly spans laterally from approximately 25.4-39.5 m and reaches at a vertical depth of about 0-6.1 m. The resistivity values range between 50-75 Ω m, which indicates a highly conductive environment consistent with leachate saturation.

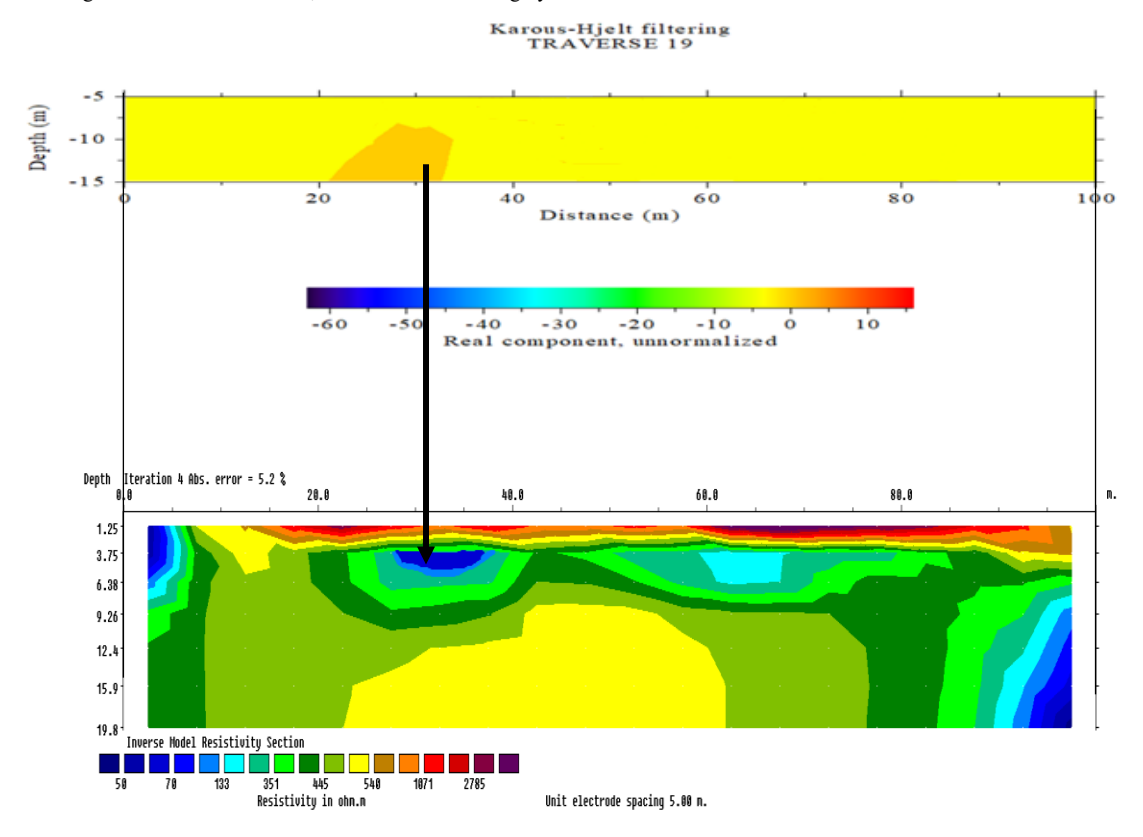


Figure 11: Correlation of VLF Conductivity and ERT Methods along Traverse 6

3. Correlation of EM-VLF and 2-D Resistivity along Traverse $7-\mbox{ Up Land}$

From the ERT and VLF results, regions of low resistivity and high conductivity signature were identified different from the surrounding soil at lateral distance of about 16-27 m, 46-48 m and 65-73m with resistivity ranging from $32.7-78\Omega$ m.

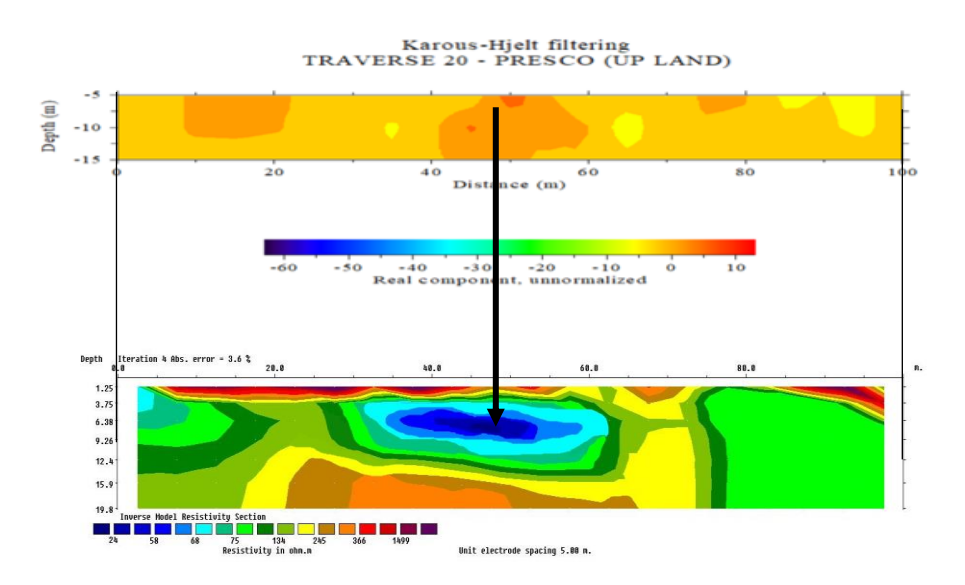


Figure 12: Correlation of VLF Conductivity and ERT Methods along Traverse 7

4. Correlation of EM-VLF and 2-D Resistivity along Traverse 14- Control

The association of the Karous-Hjelt filtered VLF data with the 2D resistivity inversion model displays a consistent and uniform subsurface feature as it does not show any impact of fertilizer pollution in the subsurface. The VLF pseudo-depth section exhibits a relatively stable yellow background tonal signal with just a few mild green patches scattered throughout (35 – 40 m, 55 –65 m, and 75 – 85 m). These anomalies, which exhibit relatively low but weak conductivity, suffered no extremes on the high conductivity side which would indicate leachate production from fertilizer contamination was seen moving through the subsurface.

The ERT resistivity section shows a clear picture of the resistivity values of the profile with relatively high to moderate subsurface resistivity values throughout the profile confirming that the subsurface consists of soils and subsurface materials that are naturally occurring and unpolluted. The resistivity values of shallow zones were approximately, $450-1700~\Omega m$ and, $2000~\Omega m$ in the deeper layers. The presence of low resistivity (<100 Ωm) features that would usually indicate leachate infiltration from the underlying fertilizer or ions accumulating for some reason was absent.

So, the consistency of the VLF and ERT results supports this interpretation given both methods suggest that this location is untouched by fertilizers. The lack of correlated conductive anomalies indicates that there is stability and no change to subsurface material, and this case, is robust as an ongoing reference or control, by which soil and subsurface materials that are impacted by fertilizers within the farmland can be compared to.

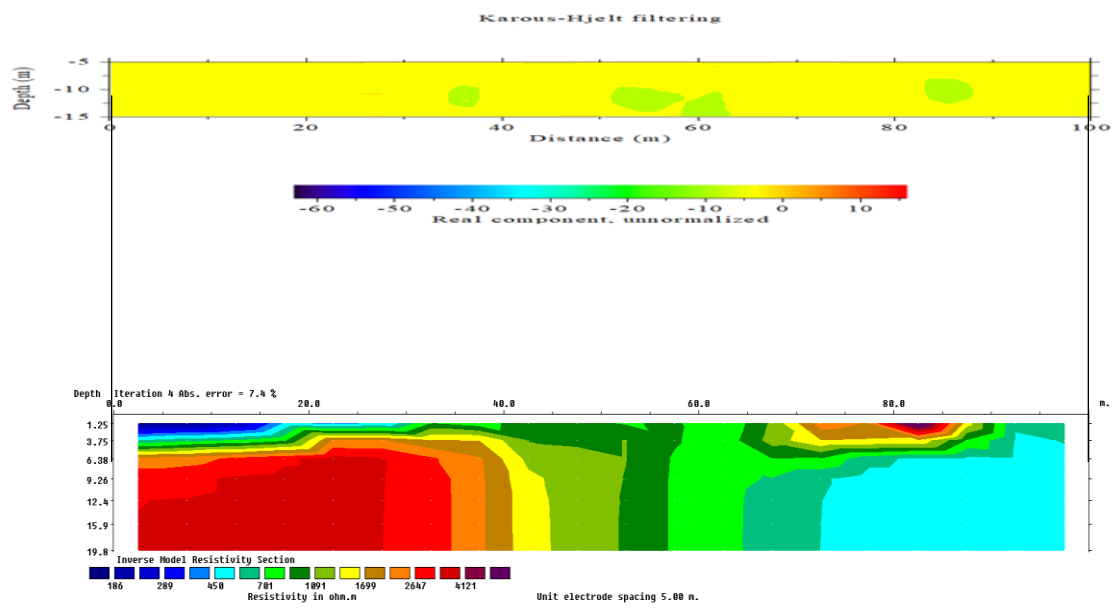


Figure 13: Correlation of VLF Conductivity and ERT Methods along Traverse 14

Discussion of Vertical Electrical Sounding (Ves) - Upland Farmland

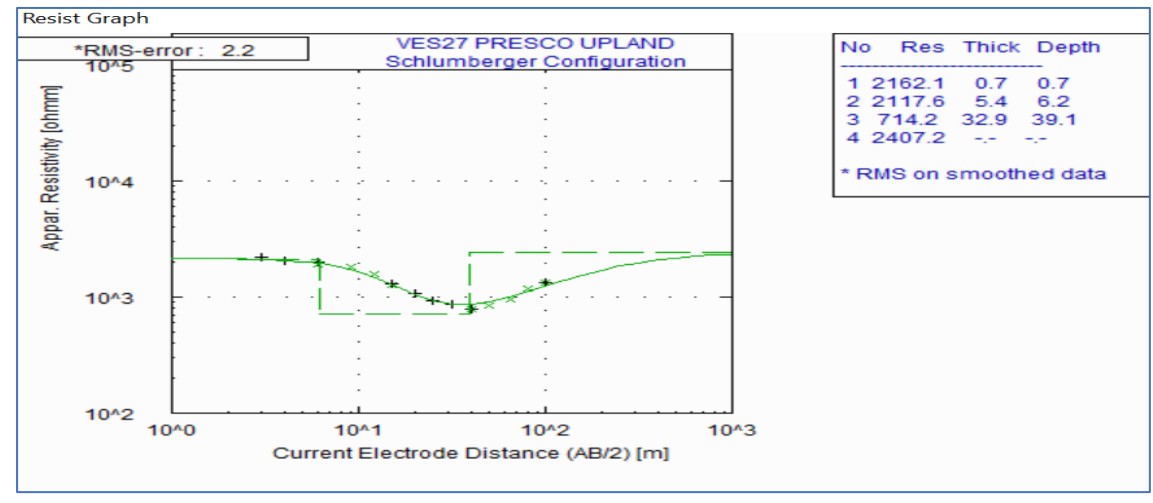


Figure 14: Resistivity Curve of VES 17 Up Land

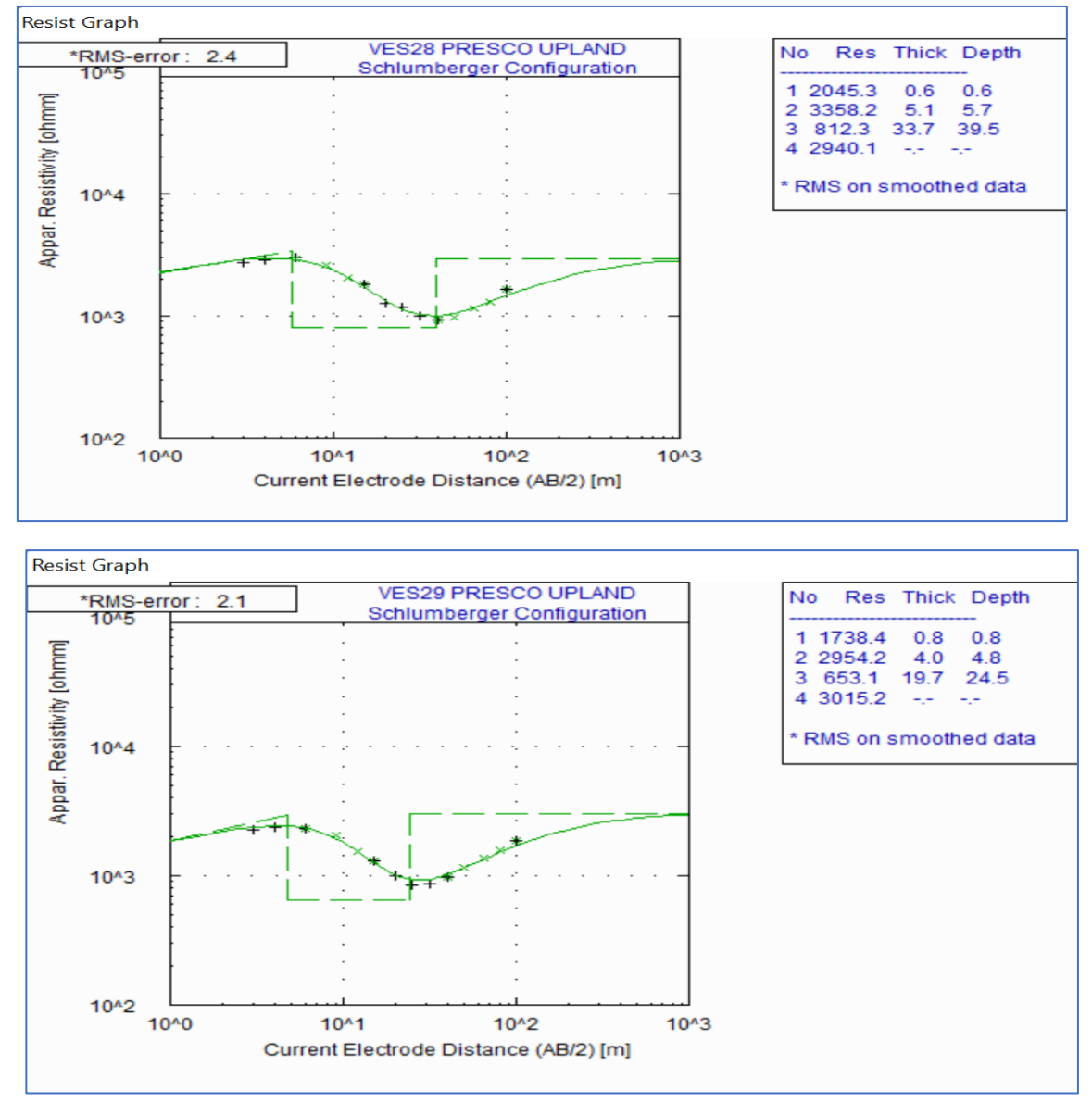


Figure 15: Resistivity Curve of VES 18 Up Land

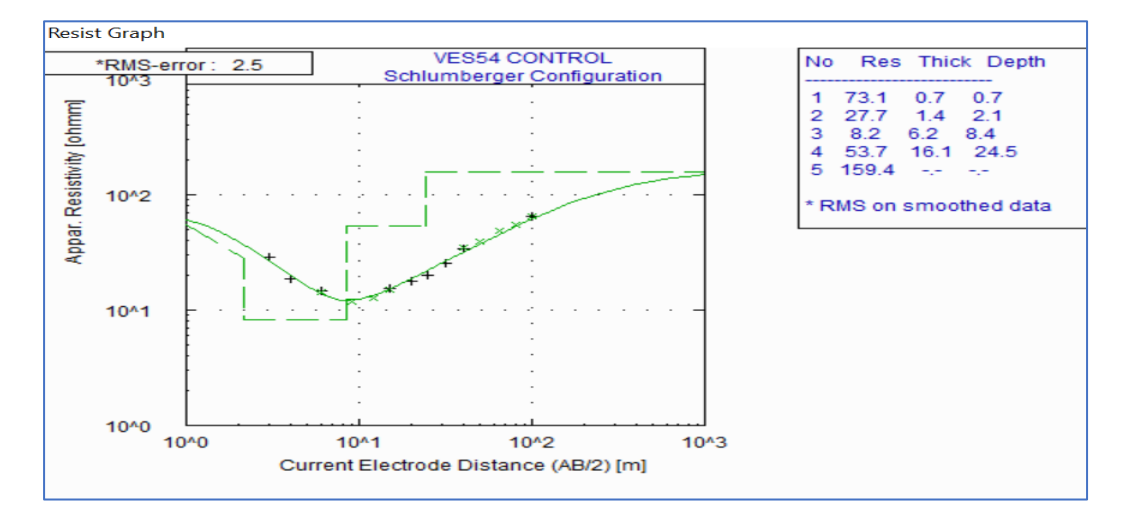


Figure 16: Resistivity Curve of VES 19 Up Land

Discussion of VES 1 - 23 (Upland)

The VES 1 to 23 reveals four to five geoelectric layers which varies from topsoil, dry sand and saturated sand. The topsoil is characterized by resistivity values ranging from $704.7 - 3019.3~\Omega m$ and layer thickness of 0.5 to 0.9 m. The second identified layer in VES (1-23) is representative of dry sand having resistivity values ranging from 1648.5 to $5696.9~\Omega m$ and layer thickness of 1.3 to 6.3 m. The third geologic unit in VES (1-3, 5-10, 13, 16-19 and 22) denotes saturated sand with resistivity and layer thickness values ranging from 355.9 to $972.5~\Omega m$ and 8.7 to 36.3~m respectively. While the saturated sand is replaced with dry sand in VES (4, 11-13, 18, 20 and 21) having resistivity values ranging from $1059.2 - 4663.3~\Omega m$ and layer thickness of 2.9 - 9.8~m. The fourth layer beneath VES (5, 6, 8, 10, 14, 16, 18, 19 and 22) depicts dry sand with resistivity values ranging from $1886.3~to~3514.5~\Omega m$ but their layer thickness could not be determined because the current terminated within this zone. While in VES (4, 7, 9, 11-13, 17, 20, 21 and 23), the dry sand is replacing with saturated sand with resistivity values ranging from $441.6 - 811.1~\Omega m$ and layer thickness of 10.6~to~38.6~m. The fifth horizon beneath VES (4, 7, 9, 11-13, 15, 17, 20, 21 and 23) is diagnostic of dry sand with resistivity values ranging from $1757.9~to~6686.5~\Omega m$ but their layer thickness could not be determined because the current terminated within the horizon.

Discussion of VES 24 (Control)

The VES 24 reveals five geoelectric layers which varies from topsoil, clay, clayey sand and saturated sand. The topsoil is characterized by resistivity values ranging from 53.4 to 73.1 Ω m and layer thickness of 0.6 to 0.7 m. The second identified layer is representative of clay having resistivity values ranging from 19.0 to 27.7 Ω m and layer thickness of 1.3 to 1.4 m. The third geologic unit denotes clay with resistivity and layer thickness values ranging from 4.9 to 8.2 Ω m and 6.2 to 6.8 m respectively. The fourth layer beneath VES 24 depicts clay sand having resistivity and layer thickness values of 53.7 Ω m and 16.1 m respectively. The fifth horizon beneath VES 24the clayey sand is replaced with saturated sand having resistivity value of 159.4 Ω m but the layer thickness could not be determined because the current terminated within this region.

3-D Horizontal Depth Slice Upland

Low-resistivity zones ($<100\,\Omega m$) appear at x: 10– $40\,m$, y: 50– $80\,m$ from 8.68– $21.9\,m$ depth, indicating deep fertilizer infiltration. The vertical trend suggests high contamination risk to the underlying aquifer.

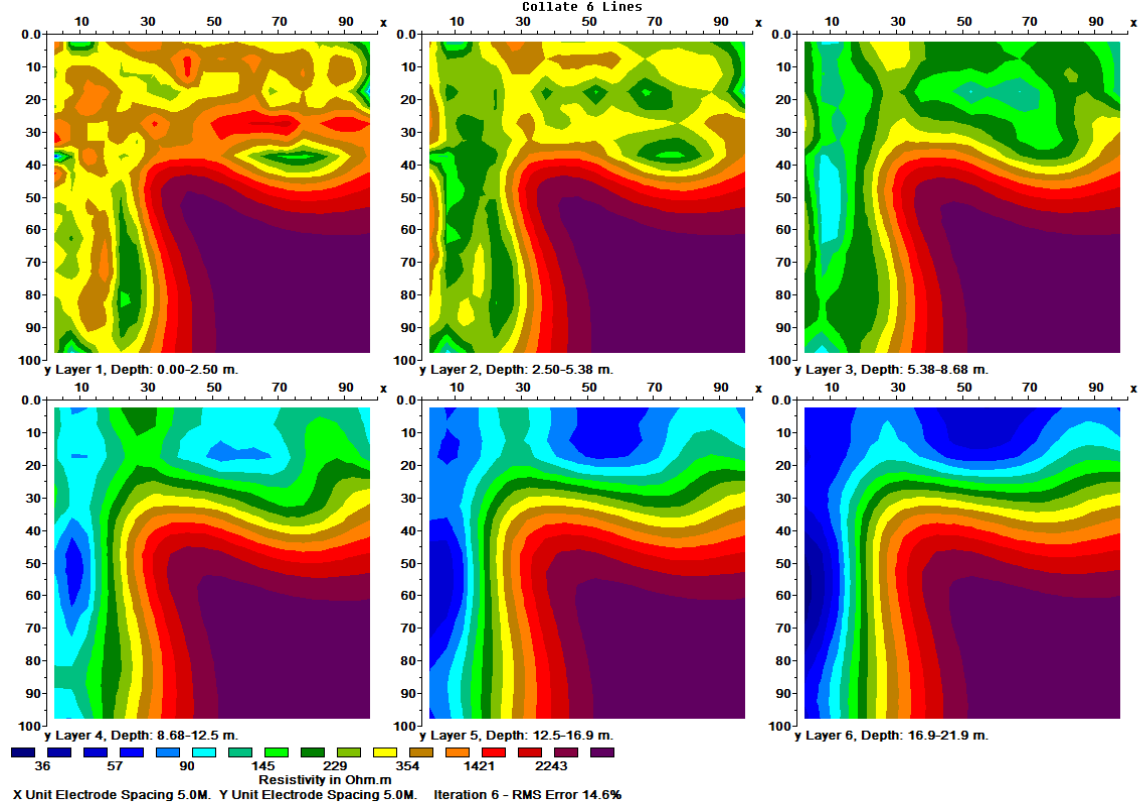


Figure 30: Horizontal Depth Slices obtained from the 3D Inversion Low Land.

Figure 18: Horizontal Depth Slices obtained from the 3D Inversion Up Land.

Figure 19: 3D inversion model of Up Land

 $Preliminary ^{1}\,Investigation; ^{1}\,Soil ^{1}\,and ^{1}\,Water ^{1}\,Analysis$

1. Water Analysis

Table 1: Upland Water Samples

S/N	Parameters	Units	Standard Methods	BOREHOLE 1 (Upland)	BOREHOLE 2 (Upland)	CONTROL	WHO Std	DPR/ NAFDAC Std
1	рН	-	ASTMD 12933- 90	5.61	5.69	6.83	6.5–8.5	6.5–8.5
2	EC	μS/cm	ASTMD 1125- 95	13	60	40	1400	1000
3	TDS	mg/L	ASTID 1868	6.7	24.5	20	1000	500
4	TSS	mg/L	ASTMD 5907- 10	<0.001	<0.001	<0.001	-	-
5	DO	mg/L	ASTMD 888-92	8.0	6.3	12.4	≥6	≥6
6	BOD	mg/L	АРНА 507	4.2	2.6	6.2	<5	<5
7	COD	mg/L	ASTMD 1252- 95	25.0	21.3	32.8	<50	<40
8	Calcium	mg/L	ASTMD 1126- 96B	6.8	10.9	4.7	75	75
9	Magnesium	mg/L	ASTMD 1126- 96B	8.1	12.5	5.8	50	50
10	Total Hardness	mg/L	ASTMD 1126- 96B	13.4	17.0	9.1	500	150
11	Sodium	mg/L	ASTMD 2791- 93	7.3	10.7	5.4	200	200

12	Potassium	mg/L	ASTMD 2791- 93	10.9	15.1	8.3	-	-
13	Alkalinity	mg/L	ASTMD 1067- 92A	31.2	42.4	22.7	100	100
14	Chloride	mg/L	API-RP-45	16.7	21.2	9.4	250	250
15	Nitrate	mg/L	АРНА 3869-90	39.75	41.29	0.68	50	50
16	Sulphate	mg/L	АРНА427С	0.91	1.18	0.82	250	100
17	Phosphate	mg/L	ASTMD 515-88	3.27	3.87	0.21	5	5
18	NH4-N	mg/L	ASTMD 1426- 15	1.61	2.0	0.07	0.5	0.5
19	Temperature	°C	EPA 1979	30.0	29.6	28.6	<35	<35
20	Iron	mg/L	ASTMD 1068- 96	0.07	0.15	0.02	0.3	0.3
21	Chromium	mg/L	API-RP-45	0.009	0.02	<0.005	0.05	0.05
22	Lead	mg/L	ASTMD 3559- 96	ND	<0.005	ND	0.01	0.01
23	Copper	mg/L	ASTMD 1188- 95	0.021	0.048	0.011	2.0	1.0
24	Zinc	mg/L	ASTMD 1691- 95	0.043	0.081	0.014	3.0	3.0
25	Nickel	mg/L	ASTMD 1886- 94	<0.005	<0.005	ND	0.02	0.02
26	Manganese	mg/L	ASTMD 858-95	0.014	0.023	ND	0.4	0.2
27	Cadmium	mg/L	ASTMD 3557- 95	ND	ND	ND	0.003	0.003

2. Soil Analysis

Table 2: Upland Soil Samples

S/N	PARAMETERS	UNITS	STANDARD	SITE		CONTROL	NIGERIAN STANDARD	WHO
			METHODS				(DPR/NAFDAC)	STD
				SAMPLE 1	SAMPLE 2			
1	рН	NA	ASTMD 12933- 90	5.34	5.28	7.20	6.5–8.5	6.5–8.5
2	EC	μs/cm	ASTMD 1125- 95	142	101	158	1000	1500
3	CALCIUM	mg/kg	ASTMD 1126- 96B	88.7	76.0	90.4	75–200	75–200

4	MAGNESIUM	mg/kg	ASTMD 1126- 96B	92.5	53.0	44.7	20–150	50
5	SODIUM	mg/kg	ASTMD 2791- 93	33.6	38.2	20.0	200	200
6	POTASSIUM	mg/kg	ASTMD 2791- 93	35.7	40.1	23.8	N/A	N/A
7	ALKALINITY	mg/kg	ASTMD 1067- 92A	52.0	50.6	48.0	20–200	100–200
8	CHLORIDE	mg/kg	API-RP-45	26.7	23.8	32.1	250	250
9	NH4-N	mg/kg	ASTMD 1426- 15	23.5	19.4	8.8	0.5	0.5
10	NITRATE	mg/kg	APHA 3869-90	19.55	20.63	0.82	50	50
11	SULPHATE	mg/kg	АРНА 427С	1.48	1.35	0.75	100-250	250
12	PHOSPHATE	mg/kg	ASTMD 515-88	2.70	2.31	1.46	5.0	5.0
13	IRON	mg/kg	ASTMD 1068- 96	90.5	76.7	38.2	0.3	0.3
14	CHROMIUM	mg/kg	API-RP-45	9.06	6.12	2.88	0.05	0.05
15	LEAD	mg/kg	ASTMD 3559- 96	5.7	3.80	ND	0.01	0.01
16	COPPER	mg/kg	ASTMD 1188- 95	20.1	16.7	3.8	1.0	2.0
17	ZINC	mg/kg	ASTMD 1691- 95	24.9	12.3	4.1	3.0	3.0
18	NICKEL	mg/kg	ASTMD 1886- 94	3.54	3.08	<0.005	0.02	0.02
19	CADMIUM	mg/kg	ASTMD 3557- 95	0.95	0.68	ND	0.003	0.003
20	MAGANESE	mg/kg	ASTMD 858-95	4.32	2.80	<0.005	0.2	0.4
21	TOTAL ORGANIC CARBON	%	ASTMD2974	1.52	1.26	0.46	N/A	N/A
22	%SAND	%	HYDROMETER	82.12	84.94	92.35	N/A	N/A
23	%SILT	%	HYDROMETER	3.38	4.80	4.05	N/A	N/A
24	%CLAY	%	HYDROMETER	14.50	10.26	3.60	N/A	N/A

CONCLUSION

The integration of electromagnetic, 1-D, 2-D and 3-D electrical resistivity geophysical methods combined with Physicochemical method were investigated to understand the level of pollution on soil and groundwater as a result of the use of fertilizers in Upland farmland in Delta State, Niger-Delta, Nigeria. The interpreted 2-D, 3-D and VES data from both locations delineated the fertilizer contaminants plume to a maximum depth of 39.6 m.The horizontal and vertical extent of fertilizer contaminants plume were both delineated by the 2-D very low frequency (VLF) and 2-D electrical resistivity imaging (ERI) as a response of the varying electrical conductivity in the fertilizer. The Physicochemical analysis revealed traces of heavy metals above the recommended WHO standards.

REFERENCES

Allred, B., Wishart, D., Martinez, L., Schomberg, H., Mirsky, S., Meyers, G., Elliot, J. and Charyton, C. (2018). Delineation of agricultural pipe patterns using ground penetration radar intehrated with a real-time kinematic global navigation satellite system. *Agriculture*, 8(167), 1-14.

Allred, B.J., Ehsani, M.R. and Daniels, J.J. (2008). Chapter 1 - general considerations for geophysical methods applied to agriculture. In: Allred BJ, Daniels JJ, Ehsani MR, editors. Handbook of Agricultural Geophysics. Boca Raton (Florida): CRC Press LLC; p. 3-16

Amato, F., Pandolfi, M., Viana, M., Querol, X., Alasfuey, A., and Moreno, T. (2009). Spatial and Chemical patterns of road dust deposited in urban environment. Atmospheric Environment43(9),1650-1659.Pergamon.http//dol.org//10.1016Jatmosenu.12008.12.009.1

Arias-Estévez, M., López-Periago, E., Martínez-Carballo, E., Simal-Gándara, J., Mejuto, J.C., García-Río, L. (2008). The mobility and degradation of pesticides in soils and the pollution of groundwater resources. Agric Ecosyst Environ 123:247-260

Ashraf, M.A., Maah, M.J. and Yusoff, I. (2014). Soil contamination, risk assessment and remediation. In: Hernandez-Soriano MC (ed) Environmental risk assessment of soil contamination. INTECH, Rijeka, 3-56

Bentley, L. R. and Gharibi, M. (2004). Resistivity Imaging at a Heterogeneous Two and Three-Dimensional Electrical Remediation Site. Geophysics, 69 (3), pp. 674 680.

Bhattacharya, A.P.K. and Patra, H.P. (1968). Direct Current Geoelectric Sounding: Principles and Interpretations: Methods of Geochemistry and Geophysics. Elsevier Publishing Company, Amsterdam. 135.

Binley, A., Hubbard, S.S, Huisman, J.A., Revil, A., Robinson, D.I., Singha, K., and Slater, L.D. (2015). The emergence of Hydrophysics for improved understanding doi:10.1002/2015WR017016. subsurface multiple processes over scales, Water Resour.Rs.,51,3837-

Black, R. (2003). Micronutrient deficiency—an underlying cause of morbidity and mortality. No. 81 (2) World Health Organization

Bradl, H.B. (2004). Adsorption of heavy metal ions on soils and soils constituents. J Colloid Interface Sci. 277(1), 1-18

Brady, N.C. and Weil, R.R. (1999). The Nature and Properties of Soils. 12th ed. Upper Saddle River (NJ): Prentice-Hall, Inc. 881.

Calace, N., Fiorentini, F., Petronio, B.M. and Pietroletti, M. (2001). Effects of acid rain on soil humic compounds. Talanta. 54:837-846

Çevre, T.C. and Orman Bakanlığı (2004). Türkiye Çevre Atlası ÇED Planlama Genel Müdürlüğü Çevre Envanteri Dairesi Başkanlığı, Ankara.

Charles, H., Godfray, J., Beddington, J.R., Crute, I.R. and Haddad, L. (2010). Food security: the challenge of feeding 9 billion people. Science 327:812-817

Chen, J. (2007). Rapid urbanization in China: a real challenge to soil protection and food security. Catena 69:1-15

Cimpoiașu, M.O., Kuras, O., Pridmore, T. and Mooney, S.J. (2020). Potential of geoelectrical methods to monitor root zone processes and structure: a review. Geoderma. 365.¹ doi:¹10.1016/j.geoderma.2020.114232.

Clair, S.B. and Lynch, J.P. (2010). The opening of pandora's box: climate change impacts on soil fertility and crop nutrition in developing countries. Plant Soil 335:101-115

Collins, M.E. and Doolittle, J.A (1987). Using Ground Penetrating Radar to study soil micro- variability, Soil Science Society of America Journal, Volume 51:491-493.

Corwin, D. L. and Lesch, S. M. (2005). "Apparent soil electrical conductivity measurements in agriculture." Computers and Electronics in Agriculture, vol. 46, pp. 11-43.

De Groot-Hedlin, C. and Constable, S.C. (1990). Occam's inversion to generate smooth two-dimensional models from magnetotelluric data. Geophysics, 55:1613-1624

Doolittle, J. A. and Brevik, E. C. (2014). The use of electromagnetic induction techniques in soil studies. Geoderma, 223(225), 33-45.

Doran, J.W. (2002). Soil health and global sustainability: translating science into practice. Agric Ecosyst Environ 88:119-127

Douaoui, A. E. K., Nicholas, H. and Walter, C. (2006). Detecting salinity hazards within a semiarid context by means of combining soil and remote sensing data. Geoderma, 134 (1-2), 217-230.

Edwards, C.A. (2002). Assessing the effects of environmental pollutants on soil organisms, communities, processes

FAO, (2009). Resource STAT-Fertilizer. Food and Agriculture Organization of the United Nations.

FAO, WHO (2014). Rome declaration on nutrition. second international conference on nutrition. Rome, Italy

Fraser, D.C. (1969). Contouring of VLF-EM Data. Geophysics, 54, 245-253.

Giller, K.E., Witter, E. and Mcgrath, S.P. (1998). Toxicity of heavy metals to microorganisms and microbial processes in agricultural soils: a review. Soil Biol Biochem. 30:1389-1414

Griffiths, D.H. and Barker, R.D. (1993). Two-dimensional resistivity imaging and modeling in areas of complex geology. Journal of Applied Geophysics, 29:211-226

Heil, K. and Schmidhalter, U. (2017). The application of EM38: Determination of soil parameters, selection of soil sampling points and use in agriculture and archaeology. Sensors, 17(11), 2540.

Iloeji, S.I. (2003). General Geography of Nigeria. Heinemann Books Ibadan. in agriculture: plant-soil continuum. Crop and Pasture Science, 66(912), 1219- 1229. DOI:10.1071/CP15104

Jadoon, K. Z., Moghadas, D., Jadoon, A., Missimer, T. M., Al-Mashharawi, S. K., and McCabe, M. F. (2015). Estimation of soil salinity in a drip irrigation system by using joint inversion of multicoil electromagnetic induction measurements. Water Resources Research, 51(5), 3490-3504.

Jayawickreme, D.H., Jobbagy, E.G. and Jackson, R.B. (2014). Geophysical subsurface imaging for ecological applications. New Phytologist. 201:1170-1175. doi:10.1111/nph.12619.

Joshua, E.O. and Mokuolu, A.O. (2016). Electrical resistivity based empirical model for delineating some selected soil properties on Sandyloam soil. Int J Sci Technol Res. 5(6):243-249.

Karlen, D. L., Andrews, S. S. and Doran, J. W. (2001). Soil quality: current concepts and applications. *Advances in Agronomy*, 74, 1-40. Karous, M.R. and Hjelt, S.E. (1983). Linear Filtering of VLF Dip—Angle Measurements. GeophysicalProspecting,31,782-894. https://doi.org/10.1111/j.1365-2478.1983.tb01085.x

Kaufmann, M. S., Von Hebel, C., Weihermüller, L., Baumecker, M., Döring, T., Schweitzer, K. and Van Der Kruk, J. (2019). Effect of fertilizers and irrigation on multi-configuration electromagnetic induction measurements. Soil Use and Management. doi:10.1111/sum.125301

Lenart-Boroń, A. and Boroń, P. (2014). The effect of industrial heavy metal pollution on microbial abundance and diversity in soils-a review. Actinomycetes, 1012, 107-108

Li, Y. and Oldenburg, D.W. (1994). Inversion of 3D DC resistivity data using an approximate inverse mapping. Geophysics Journal International, 116:527-537

Liu, H., Probst, A. And Liao, B. (2005). Metal contamination of soils and crops affected by the Chenzhou lead/zinc mine spill (Hunan, China). Sci Total Environ 339:153-166

Loke, M. and Barker, R.D. (1996a). Rapid least-squares inversion of apparent resistivity pseudo sections by a quasi-Newton method. Geophysics Prospect, 44:131–152

Loke, M.H. (2001). Electrical imaging surveys for environmental and engineering studies: a practical guide to 2D and 3D surveys, 62 pp.

Loke, M.H. and Barker, R.D. (1996b). Practical techniques for 3D resistivity surveys and data inversion. Geophysics Prospect, 44:499-524

Masindi, V. and Muedi, K. (2018). Environmental contamination by heavy metals, heavy metals. Hosam El-Din M. Saleh and Refaat F. Aglan, IntechOpen

- Mclaughlin, M.J., Tiller, K.G., Naidu, R. and Stevens, D.P. (1996). Review: the behaviour and environmental impact of contaminants in fertilizers. Aust J Soil Res 34:1-54
- Nawar, S., Corstanje, R., Halcro, G., Mulla, D. and Mouazen, A. M. (2017). Delineation of soil management zones for variable-rate fertilization: A review. Advanced Agronomy, 143, 175-245.
- Neina, D. (2019). The Role of Soil pH in Plant Nutrition and Soil Remediation. Appl. Environ. Soil Sci. 5794869
- Nishiyama, R., Ariga, A., Ariga, T., Lechmann, A., Mair, D., Pistillo, C., Scampoli, P., Valla, P. G., Vladymyrov, M., Ereditato, A. and Schlunegger, F. (2019). Bedrock sculpting under an active alpine glacier revealed from cosmicray muon radiography. Scientific Reports, 9(6970), 1-11.
- Parent, L. E. (2017). Fractal kinetics parameters regulating carbon decomposition rate under contrasting soil management systems. Open Journal of Soil Science, 7(7), 111-117.
- Pucket, G. W., Collins, M. E., and Schellentrager G.W. (1990). Using GPR for Micro-analysis of soils and karst features on the chiefland limestone plain in Florida. *Journal of Science Direct*, Vol 47,issues 1-2,pg 159-1702,DOI:10.1016/0016-7061(90)¹90053-c
- Rojas, R.V., Achouri, M., Maroulis, J. and Caon, L. (2016). Healthy soils: a prerequisite for sustainable food security. Environ Earth Sci 75, 180
- Sasaki, Y. (1992). Resolution of resistivity tomography inferred from numerical simulation. Geophysics Prospect, 40:453-464
- Shanahan, P.W., Binley, A., Whalley, W.R. and Watts, C.W. (2015). The use of electromagnetic induction to monitor changes in soil moisture profiles beneath different wheat genotypes. *Soil Science Society of America Journal*. 79:459–466. doi:10.2136/sssaj2014.09.0360.
- Shetty, P. (2009). Incorporating nutritional considerations when addressing food insecurity. Food Security 1:431-440.
- Sönmez, I., Kaplan, M. and Sönmez, S. (2007). "An investigation of seasonal changes in nitrate contents of soils and irrigation waters in greenhouses located in antalya-demre region," *Asian Journal of Chemistry*, vol. 19:7 pp. 5639-5646, 2007.
- Tahat, M., Alananbeh, K., Othman, Y. and Leskovar, D. (2020). Soil Health and Sustainable Agriculture. Sustainability. 12, 4859
- Toushmalani, R. (2010). Application of geophysical methods in agriculture. Australian Journal of Basic and Applied Sciences, 4(12), 6433-6439.
- Umeri, C. Moseri, H. and Onyemekonwu, R.C. (2016). Effects of nitrogen and phosphorus on the growth performance of maize (*Zea mays*) in selected soils of Delta State, Nigeria. *Advances in Crop Science and Technology*, 4 (1): 1-4.
- Wang, Q.R., Cui, Y.S., Liu, X.M., Dong, Y.T. and Christie, P. (2003). Soil contamination and plant uptake of heavy metals at polluted sites in China. J Environ Sci Health 38:823-838
- Whalley, W., Binley, A. and Watts, C. (2017). Methods to estimate changes in soil water for phenotyping root activity in the field. *Plant Soil*, 415, 407–422. https://doi.org/10.1007/s11104-016-3161-1
- White, S.R., Sottos, N.R., Geubelle, P.H., Moore, J.S., Kessler, M.R., Sriram, S.R., Brown, E.N. and Viswanathan, S. (2001). Autonomic healing of polymer composites. *Nature* 409: 794-797.
- Zhang, J.E., Ouyang, Y. and Ling. D.J. (2007). Impacts of simulated acid rain on cation leaching from the Latosol in south China. Chemosphere. 67:2131-2137
- Zhao, Y.F., Shi, X.Z., Huang, B., Yu, D.S., Wang, H.J., Sun, W.X., Öboern, I. and Blombäck. K. (2019). Spatial distribution of heavy metals in agricultural soils of an industry-based peri-urban area in Wuxi, China. Pedosphere.17:44-51